

Different scenarios of topological phase transitions in homogeneous neutron matter

S. S. Pankratov,¹ M. Baldo,² and M. V. Zverev^{1,3}

¹National Research Centre Kurchatov Institute, pl. Akademika Kurchatova 1, Moscow, 123182, Russia

²Istituto Nazionale di Fisica Nucleare, Sezione di Catania, 64 Via S.-Sofia, I-95123 Catania, Italy

³Moscow Institute of Physics and Technology, Institutskii per. 9, Dolgoprudnyi, Moscow region, 141700 Russia

(Dated: August 21, 2012)

We study different scenarios of topological phase transitions in the vicinity of π^0 condensation point in neutron matter. The transitions occur between the Fermi liquid state and a topologically different one with two sheets of the Fermi surface. Two possibilities of a rearrangement of quasiparticle degrees of freedom are shown: the first order topological phase transition and the second order one. The order of the phase transition is found to be strongly dependent on the value of the critical wave vector of the soft π^0 mode. The thermodynamics of the system is also studied. It is shown that the topology of the quasiparticle momentum distribution is mainly determined by the neutron matter density, while the temperature T is essential in a narrow density region. A simple explanation of the first order topological phase transition at $T = 0$ is given.

PACS numbers: 21.65.-f, 26.60.-c, 71.10.Ay

I. INTRODUCTION

A dense neutron matter is an example of the system which can exhibit strong correlations of quasiparticles (QP) degrees of freedom. The enhancement of QP interaction is revealed [1, 2] in the vicinity of π^0 condensation point (PCP) [3] where the system acquires a condensate of spin-isospin excitations with quantum numbers of the π^0 meson. The microscopic calculations [4, 5] predict the critical density value $\rho_c \simeq 0.2 \text{ fm}^{-3}$ for the PCP in neutron matter. This means that in a typical neutron star with the center density of $0.5 - 1.0 \text{ fm}^{-3}$ a significant part of stellar bulk should exist in a pion condensate phase.

The non-Fermi liquid topology of the ground state QP momentum distribution $n(p)$ in the vicinity of PCP was first uncovered in [2]. With the increase of the density ρ towards the PCP value ρ_c the QP spectrum $\varepsilon(p)$ (measured from the chemical potential μ) becomes a non-monotonic function and at certain density ρ_b manages to touch the momentum axis at some point p_b (see Fig. 1 left panel). This situation is associated with a quantum critical point (QCP) [6] at which the single particle density of states diverges [7]. Beyond the QCP, the Landau state with the Fermi step QP distribution $n_{\text{FL}}(\mathbf{p}) = \theta(p_F - p)$ becomes unstable, violating the necessary stability condition

$$\delta E[n] = 2 \int \varepsilon(\mathbf{p}, [n(\mathbf{p})]) \delta n(\mathbf{p}) dv > 0. \quad (1)$$

Here $dv = d^3\mathbf{p}/(2\pi)^3$ is the volume element in the momentum space and the factor two stands for summation over spin projections. The constraint (1) requires a positive change of the total system energy $E[n]$ for any admissible variation $\delta n(\mathbf{p})$ of the QP momentum distribution that conserves the density

$$2 \int \delta n(\mathbf{p}) dv = 0. \quad (2)$$

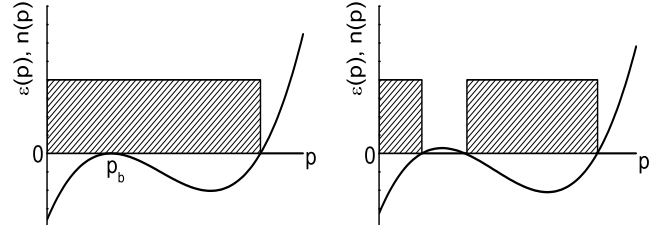


FIG. 1. Left panel: QCP at the ρ_b density value. Right panel: Beyond the QCP.

A new state appears with a "bubble" (unoccupied region) in the momentum distribution, which has several sheets of the Fermi surface (see Fig. 1 right panel). To our knowledge, such state was first discussed in [8] and the one bubble existence problem was studied in [9–11]. Further developments concerning multi-bubble states can be found in [12, 13].

All reconstructions of the QP momentum distribution in strongly correlated Fermi systems that cause a change of the Fermi surface topology are generally referred [14] as topological phase transitions (TPT). It should be noted that besides the bubble scenario, there is another type of TPT which is called the fermion condensation [15–17]. In such TPT the QP spectrum acquires a flat band $\varepsilon(p) = 0$, $p \in [p_i, p_f]$, and the Fermi surface changes its dimension. The relation between the bubble and the fermion condensation scenarios is discussed in [18].

Going back to the neutron matter problem, we stress that a bubble formation beyond the QCP is quite important for the physics of neutron stars cooling. Indeed, a new sheet of the neutron Fermi surface, with a low value of the corresponding Fermi momentum, plays an important role for an operation of the direct Urca processes: $n \rightarrow p + e^- + \bar{\nu}_e$, $p + e^- \rightarrow n + \nu_e$. In cores of neutron stars this processes are generally con-

sidered to be forbidden [19] due to the kinematic restriction for the Fermi momenta of the involving particles: $p_{F_n} \leq p_{F_p} + p_{F_e}$. In the typical density range of the core $\sim 1 - 2 \rho_0$ ($\rho_0 \simeq 0.16 \text{ fm}^{-3}$ is the normal nuclear density) the proton fraction not exceeds 6 – 8%, and the r.h.s. of the kinematic equality is estimated by $\sim 0.8 p_{F_n}$. The appearance of the new sheet of the Fermi surface at the point $p_{F_n}^{(1)} < 0.8 p_{F_n}$ allows to agree the kinematic restriction. This mechanism was considered in [2, 20] as a possibility of the enhanced cooling of some neutron stars (e.g. Vela, Geminga, 3C58).

II. QUASIPARTICLE APPROACH NEAR PION CONDENSATION POINT

A. General relations

We begin with a concise discussion of a method for describing neutron matter near the PCP. It is based on an implementation of the Landau-Migdal QP approach to strongly correlated Fermi systems that is reviewed in details [21]. The QP spectrum and the momentum distribution can be found from the set of equations:

$$\frac{\partial \varepsilon(\mathbf{p})}{\partial \mathbf{p}} = \frac{\mathbf{p}}{m} + \int f(\mathbf{p}, \mathbf{p}') \frac{\partial n(\mathbf{p}')}{\partial \mathbf{p}'} dv', \quad (3)$$

$$n(\mathbf{p}, T) = \left[1 + e^{\varepsilon(\mathbf{p})/T} \right]^{-1}, \quad (4)$$

$$2 \int n(\mathbf{p}) dv = \rho. \quad (5)$$

The first equation is the Landau relation for the QP spectrum and the interaction amplitude f in homogeneous systems. It is based on the translational invariance [22]. The quantity m is the free neutron mass. The second equation is the Fermi-Dirac statistic formula, where T is the temperature. The last one is the normalization condition including the neutron matter density ρ .

The QP interaction amplitude is identified [22] with the ω -limit of the vertex function Γ

$$\begin{aligned} f(\mathbf{p}_1, \boldsymbol{\sigma}_1; \mathbf{p}_2, \boldsymbol{\sigma}_2) &= Z^2 \Gamma_{\alpha\beta, \gamma\delta}^\omega(\mathbf{p}_1, \mathbf{p}_2) \\ &= Z^2 \cdot \lim_{\substack{k \rightarrow 0, \omega \rightarrow 0}} \Gamma_{\alpha\beta, \gamma\delta}(\mathbf{p}_1, \mathbf{p}_2, \mathbf{k}, \omega), \end{aligned} \quad (6)$$

where Z is the residue of the single particle Green function and $\boldsymbol{\sigma}_{\alpha\gamma}$ stands for Pauli spin matrices. Accord-

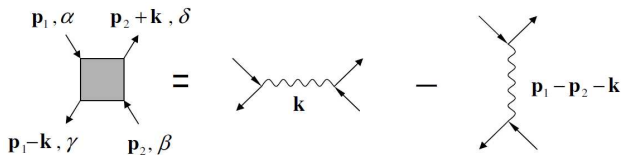


FIG. 2. The main contribution to the QP interaction amplitude.

ingly to [1], the most singular contribution to the vertex function near the PCP comes from an exchange by a soft spin-isospin collective mode. The direct and the exchange graphs of the interaction are shown in Fig. 2. After taking the $k \rightarrow 0$ limit, the contribution of the exchange graph (the second one) still shows a strong dependence on the relative momentum $\mathbf{p}_1 - \mathbf{p}_2$. Thus, the QP interaction amplitude reads [2]:

$$f(\mathbf{p}_1, \boldsymbol{\sigma}_1; \mathbf{p}_2, \boldsymbol{\sigma}_2) \simeq (\mathcal{J}_{\alpha\delta} D \mathcal{J}_{\beta\gamma})(\mathbf{p}_1 - \mathbf{p}_2, \omega = 0; \rho), \quad (7)$$

where $\mathcal{J}_{\alpha\delta}$ is the interaction vertex of nucleons and pions in neutron media, D is the π^0 propagator, and the general argument of operators is out of brackets.

B. Topological phase transitions

As it is discussed in [3], the spectrum $\omega(q)$ of π^0 -like QP excitations in neutron matter is given by a particular poles branch of the π^0 propagator. The behavior of the branch depends on the density ρ as a parameter. Pion condensation occurs at the ρ_c value when the excitation energy vanishes, $\omega(q_c) = 0$, together with its derivative, $\partial\omega(q_c)/\partial q = 0$, at a certain momentum q_c . As a consequence, at the PCP the following conditions are valid:

$$D^{-1}(q_c, 0; \rho_c) = 0, \quad \left. \frac{\partial D^{-1}(q, 0; \rho_c)}{\partial q^2} \right|_{q_c} = 0. \quad (8)$$

Using the Taylor expansion of D^{-1} in the vicinity of PCP, the interaction amplitude f , entering in Eq. (3), can be written [2, 20, 23] in the form

$$\begin{aligned} f(\mathbf{p}_1, \mathbf{p}_2) &= \frac{1}{2} \text{Sp}_{\boldsymbol{\sigma}_1} \text{Sp}_{\boldsymbol{\sigma}_2} f(\mathbf{p}_1, \boldsymbol{\sigma}_1; \mathbf{p}_2, \boldsymbol{\sigma}_2) \\ &= \frac{g}{\kappa^2(\rho) + ((\mathbf{p}_1 - \mathbf{p}_2)^2/q_c^2 - 1)^2}. \end{aligned} \quad (9)$$

Here g is an effective coupling constant and $\kappa^2(\rho) \propto (\rho_c - \rho)$ is an effective radius in momentum space. Previous investigations [23] were focused on the ground state topology, while g, q_c, κ quantities were regarded phenomenologically as free parameters. For convenience of readers, we present in Fig. 3 a topological phase diagram in q_c, κ variables obtained in that work. The label FL corresponds to the Fermi liquid state and LB_i , to states with i sheets of the Fermi surface. A change of the density ρ leads to a change of the system position (q_c, κ) on the diagram. Transitions between different regions of the phase diagram represent TPT that can happen in neutron matter. Until recently, all such TPT were considered [18, 21] to occur continuously according to violation of Eq. (1). However, it's not the only possibility and an attentive investigation [24] within the model (9) showed the existence of first order TPT. Such scenario of the Fermi surface reconstruction in a homogeneous isotropic Fermi system was first revealed [25] in a model of strongly correlated 2D electron gas beyond the QCP. Below, we present a detailed analysis of possible TPT for the neutron matter problem.

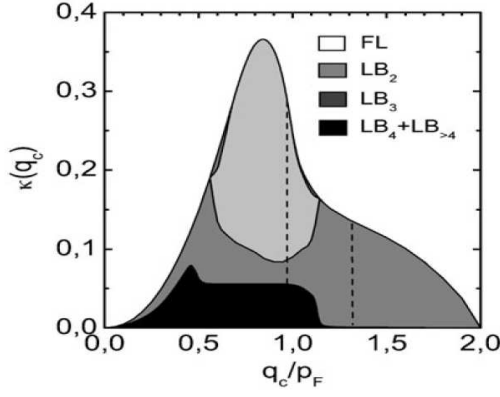


FIG. 3. The ground state neutron matter phase diagram near the PCP [23].

III. SEMI-MICROSCOPIC QP INTERACTION AMPLITUDE

The above discussion of TPT relied on the phenomenological description (9) of the QP interaction amplitude. It is possible to convey neutron matter physics near the PCP in a more direct way. A semi-microscopical expression for the QP amplitude can be derived by use of the microscopic formula (7).

The bare π^0 -nucleon interaction vertex is given [26] by

$$J_{\pi NN}^0 = \frac{if}{m_\pi}(\sigma\mathbf{q})\tau_3, \quad (10)$$

where $f \simeq 1$ is the dimensionless π^0 -nucleon coupling constant, m_π is the pion mass and τ_3 is the diagonal isospin matrix. The vertex renormalization in neutron matter is due to nucleon-nucleon correlations that can be described by means of the Landau-Migdal amplitude [27]

$$\frac{m^* p_0}{\pi^2} \mathcal{F} = F + F' \tau_1 \tau_2 + (G + G' \tau_1 \tau_2) \sigma_1 \sigma_2. \quad (11)$$

Here $p_0 = (1.5\pi^2 \rho_0)^{1/3}$ is the Fermi momentum in equilibrium nuclear matter and m^* is the effective nucleon mass. Accordingly to [3], the renormalized static vertex reads

$$J_{\alpha\beta}^{st}(\mathbf{q}) = \frac{if}{m_\pi} \frac{(\sigma_{\alpha\beta}\mathbf{q})\tau_3}{1 + g_c \chi_{NN}^{st}(q)}, \quad g_c = \frac{\pi^2}{m^* p_0} \frac{m_\pi^2}{f^2} (G + G'). \quad (12)$$

The function $\chi_{NN}^{st}(q)$ is the static susceptibility of free QP proportional to the Linhard function:

$$\chi_{NN}^{st}(q) = \frac{f^2}{m_\pi^2} \frac{m^* p_F}{\pi^2} \times \left(\frac{1}{2} + \frac{p_F}{2q} \left(\frac{q^2}{4p_F^2} - 1 \right) \ln \left| \frac{1 - q/2p_F}{1 + q/2p_F} \right| \right), \quad (13)$$

where $p_F = (3\pi^2 \rho)^{1/3}$ is the neutron Fermi momentum. The pion propagator is connected with the polarization operator: $D^{-1}(q, \omega) = \omega^2 - \mathbf{q}^2 - m_\pi^2 - \Pi(q, \omega)$. The microscopic description of the pion polarization operator is a quite subtle matter [26], and we use here the semi-microscopical representation [28]

$$\Pi(q, 0) = -q^2 \left(\frac{\chi_{NN}^{st}(q)}{1 + g_c \chi_{NN}^{st}(q)} + \frac{\rho}{\rho_\Delta (1 + q^2/q_\Delta^2)} \right). \quad (14)$$

The first term describes processes of particle-hole excitations where nucleon-nucleon correlations are taken into account by the denominator. The second term is a phenomenological one and describes Δ -resonance-hole excitations. The S -scattering processes in neutron matter are neglected. Finally, one arrives at the formula

$$f(q) = \frac{1}{2} \text{Sp}_{\sigma_1} \text{Sp}_{\sigma_2} f(\mathbf{p}_1, \sigma_1; \mathbf{p}_2, \sigma_2) = \left(\frac{f}{m_\pi} \frac{q}{1 + g_c \chi_{NN}^{st}(q)} \right)^2 \frac{1}{m_\pi^2 + q^2 + \Pi(q, 0)} \quad (15)$$

where the polarization operator is given by (14). It is worth to remark that the momentum dependence is entirely given through the relative momentum value $q = |\mathbf{p}_1 - \mathbf{p}_2|$.

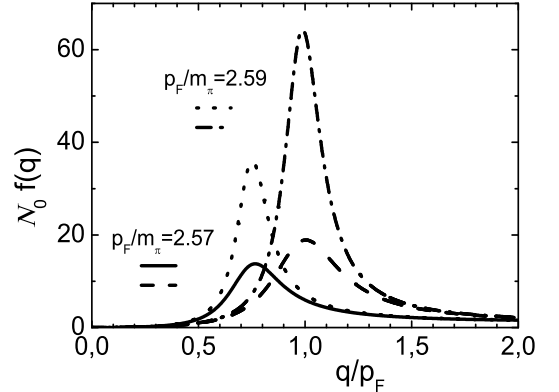


FIG. 4. The interaction amplitude (15) multiplied by $N_0 = mp_F/\pi^2$ as a function of q/p_F . The parametrization (16) corresponds to curves peaked at $q_c \simeq 0.74 p_F$, while (17), at $q_c \simeq p_F$.

We now discuss the parameters entering the amplitude $f(q)$. The constants: $f = 1$, $m^* = m$, $G + G' = 1$ are fixed all along the further discussion, while we use two sets of parametrizations for the phenomenological part of the polarization operator. The first one corresponds to the choice in [28], where

$$\rho_\Delta = 0.59 m_\pi^3, \quad q_\Delta = 2.08 m_\pi. \quad (16)$$

The second parametrization is suggested in this work:

$$\rho_\Delta = 0.97 m_\pi^3, \quad q_\Delta = 4.1 m_\pi. \quad (17)$$

Each parametrization reproduces the value $\rho_c \simeq 0.2 \text{ fm}^{-3}$ that agrees with the critical density of π^0 condensation obtained in [4, 5]. The difference is in the corresponding value of the critical wave vector q_c , which is not known well from microscopic calculations. We also note that ρ_c and q_c are quite sensitive to the tuning of ρ_Δ and q_Δ parameters. The behavior of the QP interaction amplitude is shown in Fig. 4. The parametrization (16) leads to $q_c \simeq 0.74 p_F$ (that is less than p_F), while (17), to $q_c \simeq p_F$. Fig. 4 also demonstrates the amplification of the amplitude with an increase of the p_F value (or the density $\rho = p_F^3/3\pi^2$). The real divergence, that is exactly at the PCP, is reached at the point $p_F \simeq 2.602 m_\pi$ and $p_F \simeq 2.598 m_\pi$ correspondingly for the first and the second parametrizations.

IV. DIFFERENT SCENARIOS OF TOPOLOGICAL PHASE TRANSITIONS

Here we present the results for topological rearrangements of QP degrees of freedom based on the semi-microscopical QP interaction amplitude. The associated TPT are considered with respect to the density and the temperature changes and turns out to be of first or second order depending on π^0 polarization operator parameters (finally on the q_c value).

The QP spectrum and the momentum distribution are determined by the set of equations (3),(4),(5). The first equation permits an integration by parts, due to the assumed dependence (15) on the relative momentum q of the interaction amplitude

$$\varepsilon(\mathbf{p}) = \frac{p^2}{2m} - \mu + \int f(\mathbf{p} - \mathbf{p}') n(\mathbf{p}') dv'. \quad (18)$$

Then, it is convenient to apply a contracting iterations method for the solution of this set of equations. The case of $T = 0$ (when it is addressed) was modeled by $T = 10^{-5} \varepsilon_F^0$, where $\varepsilon_F^0 = p_F^2/2m$.

First, we consider the results obtained within the model (16) where $q_c \simeq 0.74 p_F$. The corresponding QP degrees of freedom evolution, driven by an increase of p_F , is displayed in Fig. 5. It has a continuous behavior according to the QCP scenario of the Fermi surface reconstruction. At the critical value $p_F^b = 2.562 m_\pi$ a bifurcation occurs, and a new root of the QP spectrum appears at the point $p_b = 0$. Beyond the QCP, the QP momentum distribution possesses two sheets of the Fermi surface with coordinates p_1 and $p_2 \simeq p_F$. The bubble region size (which is equal to p_1) increases continuously from the zero value with the further increase of p_F .

Regarding Eq. (18), it is easy to write down the corresponding energy functional

$$E[n] = 2 \int \frac{p^2}{2m} n(\mathbf{p}) dv + \int f(\mathbf{p} - \mathbf{p}') n(\mathbf{p}) n(\mathbf{p}') dv dv'. \quad (19)$$

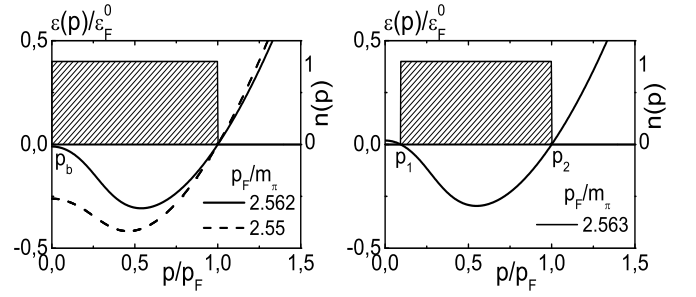


FIG. 5. The QP spectrum (in units $\varepsilon_F^0 = p_F^2/2m$) and the momentum distribution evolution with the increase of p_F within the model (16). The temperature $T = 0$.

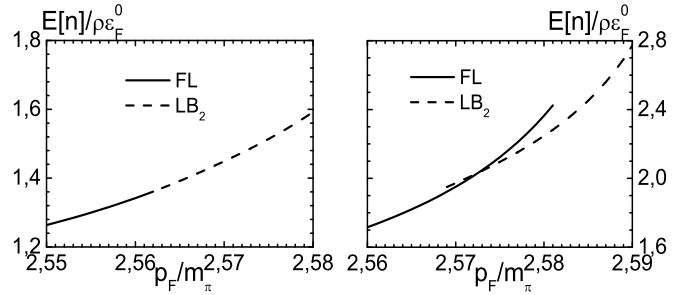


FIG. 6. Energy per particle at $T = 0$ as a function of p_F . Left panel corresponds to the model (16), while right one, to the model (17).

According to the continuous picture of the ground state evolution (Fig. 5), the energy shows a monotonic behavior as it is plotted on the panel of Fig. 6. The topological transition between the FL and the LB_2 states is of the second order.

Now, we turn to the model (16) where $q_c \simeq p_F$. Let us first consider the right panel of Fig. 6. It is seen that there are two different states in the interval $2.57 m_\pi \lesssim p_F \lesssim 2.58 m_\pi$. We note that in order to establish the coexistence of several solutions of the equations (4),(5),(18) it is steadily necessary [24, 25] to consider different initial conditions for the iteration procedure. Fig. 7 represents QP spectra and momentum distributions of coexisting states. At the value $p_F = 2.572 m_\pi$ the ground state is the FL one (panel (a)), while there is also a LB_2 state (panel (b)) with a slightly higher energy value (see the right panel of Fig. 6). It is worth to emphasize that the bubble region has finite, not negligible size $p_1 \simeq 0.6 p_F$. A first order phase transition takes place at the $p_F \simeq 2.573 m_\pi$ value. Beyond the transition point, the LB_2 state (panel (d)) becomes energetically favored over the FL state (panel (c)). Finally, the local energy minimum of the functional (19), corresponding to the FL state, becomes unstable [29] (for $p_F \gtrsim 2.581 m_\pi$) and only the LB_2 ground state remains (the right panel of Fig. 6).

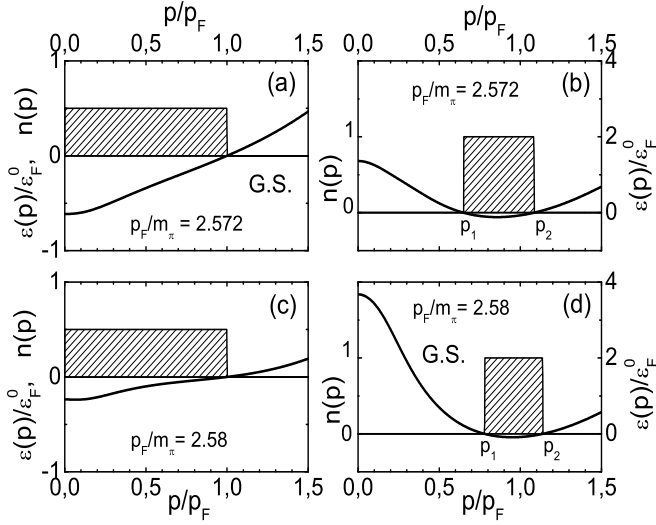


FIG. 7. Panels (a), (b): QP spectra and momentum distributions of coexisting states in advance of the first order TPT. Panels (c), (d): the same, beyond the TPT point. The temperature $T = 0$.

Thermodynamic functions of neutron matter with the Fermi momentum $p_F = 2.572 m_\pi$ are given by Fig. 8. The panel (a) demonstrates that the FL state is lower in the energy then the LB_2 one up to the temperature $T \sim 0.1 \varepsilon_F^0 \sim 5 \text{ MeV}$. At the same time, the panel (b) shows that the entropy value

$$S[n] = -2 \int n(\mathbf{p}) \log n(\mathbf{p}) + (1 - n(\mathbf{p})) \log(1 - n(\mathbf{p})) dv, \quad (20)$$

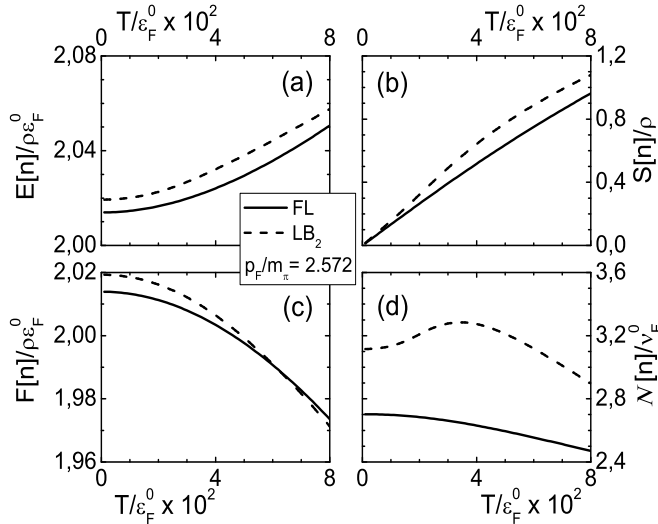


FIG. 8. The energy (panel (a)), the entropy (panel (b)), the free energy (panel (c)) and the density of states (panel (d)) as functions of the temperature for the FL and the LB_2 states.

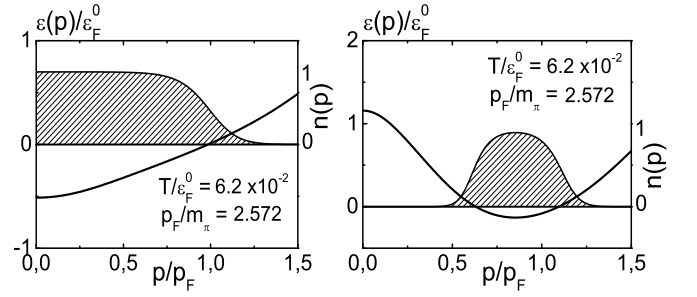


FIG. 9. QP spectra and momentum distributions of the FL and the LB_2 states at the point (the black dot A in Fig. 10 below) of the temperature driven TPT.

corresponding to the LB_2 state, grows more rapidly as the temperature increases, than the one of the FL state. An interplay of the energy and the entropy balance leads to a first order TPT that is driven by the temperature. The free energy $F[n] = E[n] - TS[n]$ behavior is given by the panel (c) and demonstrates the phase transition at the temperature $T_1 \simeq 6.2 \cdot 10^{-2} \varepsilon_F^0$. Finally, the panel (d) shows the density of states

$$\mathcal{N}[n] = \int \frac{dn(\mathbf{p})}{d\varepsilon} dv = \frac{1}{T} \int n(\mathbf{p})(1 - n(\mathbf{p})) dv. \quad (21)$$

To elucidate the temperature dependence, we present in Fig. 9 QP spectra and momentum distributions of the FL state and the LB_2 one at the point $T = 6.2 \cdot 10^{-2} \varepsilon_F^0$ near the phase transition. Thus, the higher values of the entropy and the density of states, corresponding to the LB_2 state, are caused by "melting" of two sheets of the Fermi surface, while the FL state has only one sheet.

The temperature investigations of the QP states behavior, in the region near the point $p_F = 2.572 m_\pi$ (see the right panel of Fig. 6), are gathered by a (p_F, T) -phase

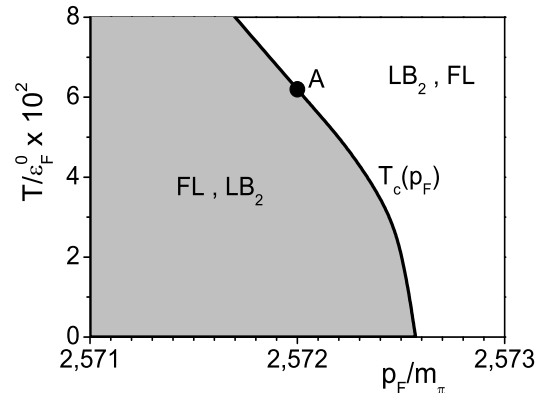


FIG. 10. Phase diagram of neutron matter near the line $T_1(p_F)$ of the first order TPT. The first label corresponds to the thermodynamically favored phase, the second one, to a metastable phase. The black dot A refers to the QP states shown in Fig. 9.

diagram of neutron matter shown in Fig. 10. The diagram consists of two regions: the first one corresponds to the FL phase of the system, while the other one, to the LB_2 phase. The regions are separated by the line $T_1(p_F)$ of the first order TPT. The diagram shows that neutron matter state topology is determined by the temperature in a quite narrow density interval.

V. ENERGETICS OF LB_2 STATES

In this section, we elucidate why the system appears to be in the LB_2 phase. The energy functional (19) can be rewritten in the form

$$E[n] = 2 \int \frac{p^2}{2m} n(\mathbf{p}) dv + \frac{1}{2} \int f(\mathbf{q}) S(\mathbf{q}; [n]) dv. \quad (22)$$

Here the interaction energy part is given by use of the structure function

$$S(\mathbf{q}; [n]) = \frac{2}{\rho} \int n(\mathbf{p} + \mathbf{q}) n(\mathbf{p}) dv. \quad (23)$$

Then, we address below the case of $T = 0$. The set of all possible QP momentum distributions with one or two sheets of the Fermi surface (that is the FL or LB_2 states) is specified by

$$n_2(\mathbf{p}) = \theta(p_2 - p) - \theta(p_1 - p), \quad (24)$$

$$p_2^3 - p_1^3 = p_F^3. \quad (25)$$

The last equation follows from the normalization condition (5). This class is referred below as n_2 type QP distributions. In this case, the structure function is evaluated explicitly, the corresponding formulas are given in the Appendix. It is sufficient, due to (25), to deal with one parameter. The convenient choice is $\eta = p_2 - p_1$ (the width of the occupied region in the QP momentum distribution) that defines distribution parameters

$$p_{1,2} = \frac{1}{\sqrt{3}} \sqrt{\frac{p_F^3}{\eta} - \left(\frac{\eta}{2}\right)^2} \mp \frac{\eta}{2}. \quad (26)$$

The value $\eta = p_F$ corresponds to $p_1 = 0$, $p_2 = p_F$ (the Fermi step). The decrease of η leads to a monotonic increase of $p_{1,2}$.

The behavior of the structure function $S(\mathbf{q}; [n_2]) = S(q; \eta)$ is shown by Fig. 11 (the left panel).

Its explicit form corresponding to the Landau state ($\eta = p_F$), is well known

$$\begin{aligned} S(q; p_F) &= S_{FL}(q) \\ &= \frac{1}{2} \left(1 - \frac{q}{2p_F}\right)^2 \left(2 + \frac{q}{2p_F}\right) \theta(2p_F - q). \end{aligned} \quad (27)$$

It is remarkable that in the other important case of thin ($\eta \ll p_F$) n_2 type QP distributions that can appear by a first order TPT, one obtains

$$S(q; \eta)|_{\eta \rightarrow 0} = \frac{\eta}{2q}. \quad (28)$$

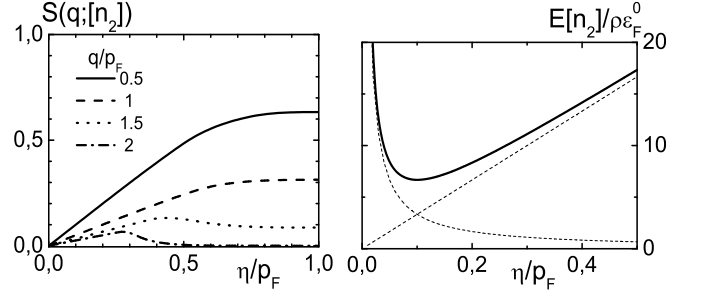


FIG. 11. Left panel: The structure function of the n_2 type QP momentum distributions. Several values of the wave vector q are regarded. Right panel: The total energy per particle for the thin n_2 type momentum distributions.

This result is demonstrated well by Fig. 11, and reflects the natural decrease of the momentum distributions overlap in the integral of Eq. (23). As a consequence, this leads to a reduction of the interaction energy value

$$E_{int}[n_2]|_{\eta \ll p_F} \simeq \frac{U\eta}{2p_F}, \quad U = p_F \int \frac{f(q)}{2q} dv. \quad (29)$$

The kinetic energy, on the contrary, shows enhancement that is confirmed by the explicit result

$$\begin{aligned} E_{kin}[n_2] &= \frac{3}{5p_F^5} (p_2^5 - p_1^5) \epsilon_F^0 \rho \\ &= \left(\frac{p_F}{3\eta} + \frac{\eta^2}{3p_F^2} - \frac{\eta^5}{15p_F^5} \right) \epsilon_F^0 \rho. \end{aligned} \quad (30)$$

The total energy value of n_2 type distributions in the limit $\eta \ll p_F$ is given by

$$E[n_2] \simeq \left(\frac{p_F}{3\eta} + \frac{u\eta}{2p_F} \right) \epsilon_F^0 \rho, \quad u = U/\epsilon_F^0 \rho. \quad (31)$$

This function is plotted on Fig. 11 (the right panel) and reveals an evident minimum, that is

$$E_{LB_2} = \sqrt{\frac{2}{3}} u \epsilon_F^0 \rho \quad (32)$$

at the width value $\eta_c = p_F \sqrt{2/(3u)}$. Finally, we note that the E_{LB_2} energy value appears to be lower the Fermi liquid one

$$E_{FL} = \frac{3}{5} \epsilon_F^0 \rho + \frac{1}{2} \int f(q) S_{FL}(q) dv, \quad (33)$$

when the QP interaction is sufficiently strong. Indeed, if one characterizes the QP interaction amplitude by an effective coupling constant $f(q) \propto g$, equations (32) and (33) show $E_{LB_2} \propto \sqrt{g}$ and $E_{FL} \propto g$ behavior at the large g limit.

Thus, the appearance of LB_2 states is explained by the interplay between the kinetic and the interaction energy

contributions. The existence of this energy minimum, generally, does not depend on whether the Landau state is present or not. We remark that this simple explanation is limited by the n_2 set of QP momentum distributions. A generalization to a more complete class $n_{\alpha>2}$ could in principle reveal an instability of a LB_2 state with respect to some energetically favored one [24]. The solid proof of the existence of the LB_2 ground state comes from the direct solution of the equations (4),(5),(18).

VI. CONCLUSION

In this article we have considered two scenarios of topological phase transitions in homogeneous neutron matter. The transitions occur between the Fermi liquid state and the other one with two sheets of the Fermi surface. The investigation was performed with the use of a semi-microscopical expression for the quasiparticle interaction amplitude in the vicinity of π^0 condensation point. The order of the phase transition is confirmed to be strongly dependent on the critical wave vector q_c in agreement with more simplified formulations [24]. The first possibility for a rearrangement of the quasiparticle degrees of freedom is the second order topological phase transition. It occurs when $q_c < p_F$, and it corresponds to a quantum critical point scenario [6, 7, 18] of the Fermi surface reconstruction. The second possibility studied in this work is the first order topological phase transition. This case occurs when $q_c \gtrsim p_F$ and it is connected with a sudden change in the quasiparticle momentum distribution and spectrum. The first order topological phase transition can be driven either by the density or the temperature changes. Thermodynamic functions and the phase diagram are calculated. It is shown that the influence of the temperature on the Fermi surface topology is essential in a quite narrow density region. A simple explanation of the origin of the first order topological phase transition at $T = 0$ is given.

VII. ACKNOWLEDGMENTS

We thank V. A. Khodel and E. E. Saperstein for their interest to this work and useful discussions. One of the authors (S.S.P.) would like to thank INFN (Sezione di Catania) for hospitality during his stay in Catania. This research was partially supported by the Grants # NSh-7235.2010.2 and # 2.1.1/4540 of the Russian Ministry for Science and Education, and by the RFBR Grants 11-02-00467-a and 12-02-00955-a.

VIII. APPENDIX

The structure function within the n_2 set of QP momentum distributions reads

$$S(\mathbf{q}; [n_2]) = \frac{2}{\rho} \int n(\mathbf{p} + \mathbf{q})n(\mathbf{p}) dv = S_{11} + S_{22} - 2S_{12}. \quad (34)$$

Here $(4\pi/3)p_F^3 S_{ij}$ is a volume of two spheres intersection with radii $p_{\min} = p_i$ and $p_{\max} = p_j$, $p_{\min} \leq p_{\max}$, while the distance between the centers is equal the \mathbf{q} vector length. The value of the volume is specified by

$$p_F^3 S_{ij}(q; p_i, p_j) = (\zeta(q; p_i, p_j) + \zeta(q; p_j, p_i)) \times \theta(p_i + p_j - q)\theta(q + p_i - p_j) + p_i^3 \theta(p_j - q - p_i). \quad (35)$$

The first term corresponds to an intersection case, while the second one, to a complete enclosure of the small sphere into the bigger one. The function ζ has the form

$$\zeta(q; p_i, p_j) = \frac{1}{4} \left(p_i - \frac{p_i^2 + q^2 - p_j^2}{2q} \right)^2 \times \left(2p_i + \frac{p_i^2 + q^2 - p_j^2}{2q} \right). \quad (36)$$

-
- [1] A. M. Dyugaev, Zh. Eksp. Teor. Fiz. **70**, 2390 (1976) [Sov. Phys. JETP, **43**, 1247 (1976)].
 - [2] D. N. Voskresensky, V. A. Khodel, M. V. Zverev and J. W. Clark, The Astrophysical Journal **533**, 127 (2000) [arXiv:astro-ph/0003172].
 - [3] A. B. Migdal, Rev. Mod. Phys. **50**, 107 (1978).
 - [4] R. B. Wiringa, V. Fiks and A. Fabrocini, Phys. Rev. C **38**, 1010 (1988).
 - [5] A. Akmal, V. R. Pandharipande and D. G. Ravenhall, Phys. Rev. C **58**, 1804 (1998) [arXiv:nucl-th/9804027]. A. Akmal, V. R. Pandharipande, Phys. Rev. C **56**, 2261 (1997) [arXiv:nucl-th/9705013].
 - [6] V. A. Khodel, Pis'ma v ZhETP **86**, 832 (2007) [arXiv:0709.3653].
 - [7] V. A. Khodel, J. W. Clark, M. V. Zverev, Pis'ma v ZhETP **94**, 73 (2011) [arXiv:1105.2552].
 - [8] H. Fröhlich, Phys. Rev. **79**, 845 (1950).
 - [9] M. de Llano, J. P. Vary, Phys. Rev. C **19**, 1083 (1979).
 - [10] M. de Llano, A. Plastino, J. G. Zabolitzky, Phys. Rev. C **20**, 2418 (1979).
 - [11] V. C. Aguilera-Navarro, R. Barrera, M. de Llano, J. W. Clark, A. Plastino, Phys. Rev. C **25**, 560 (1982).
 - [12] M. V. Zverev and M. Baldo, JETP **87**, 1129 (1998) [arXiv:cond-mat/9807324].
 - [13] S. A. Artamonov, Yu. G. Pogorelov, V. R. Shaginyan, Pis'ma v ZhETP **68**, 893 (1998) [arXiv:cond-mat/9811024].
 - [14] G. E. Volovik, Springer Lecture Notes in Physics **718**, 31 (2007).
 - [15] V. A. Khodel and V. R. Shaginyan, JETP Lett. **51**, 553 (1990).
 - [16] G. E. Volovik, JETP Lett. **53**, 222 (1991).
 - [17] P. Nozières, J. Phys. I France **2**, 443 (1992).
 - [18] V. A. Khodel, J. W. Clark, M. V. Zverev, Phys. Rev. B **78**, 075120 (2008) [arXiv:0806.1908].

- [19] P. Haensel, A. Y. Potekhin, D. G. Yakovlev, *Neutron Stars 1, Equation of State and Structure*, Springer Astrophysics and Space Science Library **326**, (2007).
- [20] V. A. Khodel, J. W. Clark, M. Takano and M. V. Zverev, Phys. Rev. Lett. **93**, 151101 (2004).
- [21] V. A. Khodel, J. W. Clark, M. V. Zverev, Phys. Atom. Nucl. **74**, 1237 (2011) [arXiv:1108.4023].
- [22] A. A. Abrikosov, L. P. Gor'kov, I. E. Dzyaloshinski, *Methods of Quantum Field Theory in Statistical physics*, London: Prentice-Hall, 1963.
- [23] M. Baldo, V. V. Borisov, J. W. Clark, V. A. Khodel and M. V. Zverev, J. Phys.: Condens. Matter **16**, 6431 (2004) [arXiv:cond-mat/0402481].
- [24] S. S. Pankartov, M. V. Zverev, JETP Letters, to be published.
- [25] S. S. Pankartov, M. V. Zverev, M. Baldo, JETP Letters **93**, 591 (2011) [arXiv:1106.5160].
- [26] T. Ericson, W. Weise, *Pions and Nuclei*, Oxford: Clarendon Press, 1988.
- [27] A. B. Migdal, *Theory of Finite Fermi Systems and Applications to Atomic Nuclei*, New York: Wiley, 1967.
- [28] A. B. Migdal, O. A. Markin, and I. I. Mishustin, Zh. Eksp. Teor. Fiz. **66**, 443 (1974) [Sov. Phys. JETP, **39**, 212 (1974)].
- [29] Detailed analysis of the energy functional (19) with a QP interaction amplitude of the form (9) can be found in [24] for nuclear matter and in [25] for 2D electron gas problems.